Nanomechanics of the molecular complex between staphylococcal adhesin SpsD and elastin

Marion Mathelié-Guinlet[1], Constance Chantraine[1], Felipe Viela[1], Giampiero Pietrocola[2], Pietro Speziale[2], and Yves F. Dufrêne[1,3]

[1]Louvain Institute of Biomolecular Science and Technology, UCLouvain, Croix du Sud, 4-5, bte L7.07.07, B-1348 Louvain-la-Neuve, Belgium

[2]Department of Molecular Medicine, Unit of Biochemistry, University of Pavia, Viale Taramelli 3/b, 27100 Pavia, Italy

[3]Walloon Excellence in Life sciences and Biotechnology (WELBIO), B-1300 Wavre, Belgium

[*]Corresponding authors:

Yves Dufrêne: yves.dufrene@uclouvain.be

Pietro Speziale: pspeziale@unipv.it

Keywords: staphylococci, SpsD, elastin, single-molecule, mechanostability, ultrastrong binding

Abstract

Staphylococcus pseudintermedius surface protein SpsD binds to extracellular matrix proteins to invade canine epithelial cells. Using single-molecule experiments, we show that SpsD engages in two modes of interaction with elastin that are tightly controlled by physical stress. Binding is weak (~100 pN) at low tensile force (*i.e.* loading rate), but is dramatically enhanced (up to ~1,500 pN) by mechanical tension. Consistent with a "dock, lock, and latch" (DLL) mechanism, this force represents among the highest mechanical strength known for a non-covalent biological interaction. The transition from weak to strong binding correlates with an increase in molecular stiffness but, surprisingly, with a decrease in molecular extension. This unanticipated, counterintuitive mechanical behavior indicates that the adhesin is engaged in two distinct interaction mechanisms. Our results emphasize the crucial role of protein nanomechanics in the adhesion of staphylococci, and illustrate their wide diversity of force-dependent ligand-binding activities. These single-molecule mechanical experiments may contribute to the development of antiadhesion approaches to treat infections caused by *S. pseudintermedius* and other bacterial pathogens engaged in DLL interactions.

Staphylococcus pseudintermedius is a commensal pathogen of domestic animals, notably responsible of canine bacterial infections, such as pyoderma and otitis. The increasing occurrence of methicillin-resistant *S. pseudintermedius* strains [1,2] and the recognized transmission to humans [3] have raised a worldwide concern and an urgent need to understand their virulence. It is well-established that *S. pseudintermedius* has evolved a plethora of surface proteins, similarly to other staphylococci, that promote host cell invasion and interactions with proteins of the extracellular matrix (ECM), such as fibrinogen (Fg), fibronectin (Fn) and elastin [4,5]. Among them, SpsD and SpsL have many common features with the typical staphylococcal MSCRAMMs (for microbial surface components recognizing adhesive matrix molecules) proteins [6] - mainly a N-terminal comprising an A-domain (Fig. 1) homologous to the A domains of clumping factors (Clfs) and Fn-binding proteins (FnBPs) of *S. aureus* which are known to bind to the above-mentioned ECM proteins [7]. An interesting trait of SpsD is its multi-ligand binding properties, being able to interact with Fg, Fn, elastin and cytokeratin 10 [7]. SpsD and SpsL use these interactions for skin colonization and infection [7,8], especially through the binding to Fn which bridges the bacterial surface with specific integrins in the host cell membrane [9]. The pathogen might also attach to elastin, which makes up the highly insoluble amorphous component of elastic fibers in the extracellular space of many tissues such as lung, dermis and large blood vessels. Elastin provides elastic tissues, like skin, with resilience to a variety of forces [10,11]. This complex protein consists in the cross-linking assembly of tropoelastin monomers (~72 kDa), molecular nanosprings of about 20 nm long, that coacervate to form large elastin fibers [12]. Several pathogens, such as *Mycobacterium tuberculosis* and *Leptospira spp.,* have been demonstrated to bind elastin and tropoelastin [13,14]. In *S. aureus*, it was initially shown that the membrane-associated protein EbpS promotes binding of soluble elastin peptides and tropoelastin to the bacteria and suggested that EbpS

might be the adhesin responsible for the bacterial colonization of elastin-rich tissues [15,16]. In a later study, a major role as elastin-binding protein was attributed to FnBPA and FnBPB [17,18]. The binding site for elastin was localized to subdomains N2-N3 of the A domain of *S. aureus* FnBPA, which is also the binding site for the Fg γ-chain. This interaction, being inhibited by a peptide comprising the C-terminus of the Fg γ-chain, likely occurs through the "dock, lock and latch" (DLL) mechanism [19] firstly proposed for the binding of the *S. epidermis* adhesin SdrG to the Fg β –chain [20]. Such mechanism highly strengthens the receptor-ligand bond, subsequently increasing the firm attachment of the pathogen to the host cell.

SpsD has also been reported to bind elastin and Fg through its N2-N3 subdomains, likely through the DLL mechanism or a variant of it [7], but the underlying molecular details are currently unknown. By means of single-molecule atomic force microscopy (AFM) experiments [21], we investigate the forces involved in the binding of SpsD to elastin and the dynamical behavior of such bonds. We find that SpsD and elastin form molecular complexes with unexpected mechanical properties. They bind through both weak, long-range interactions and strong, short-range interactions. Consistent with a DLL mechanism, strong binding is favored by tensile force. Also, the increase in binding strength correlates with an increase in molecular stiffness but with a decrease in molecular extension. This previously undescribed behavior shows that the adhesin is engaged in a dual interaction mechanism.

Results

SpsD binds to elastin through both weak and strong forces. We investigated *S. pseudintermedius* ED99 strains *ΔspsL* and *ΔspsD* expressing only SpsD or SpsL respectively (hereafter SpsD and SpsL cells). By means of force spectroscopy with elastin-modified tips, the strength of single SpsD-elastin interactions was measured on living bacteria. Fig. 2A-B show

the adhesion forces and rupture lengths obtained for three representative cells (for more cells see Table 1). Force curves featured adhesion events with both weak (< 500 pN) and strong (> 500 pN) forces, to an extent that varied from one cell to another. Analysis of the force profiles over 14 cells yielded an average force of 207 ± 57 pN in the low regime (*n* = 5,191 total adhesive curves), while the high regime exhibited a mean of 1,048 ± 204 pN (*n* = 4048 total adhesive curves) (Fig. 2B inset; Table 1). We note that there were substantial variations in adhesion forces from one cell to another, an effect that we attribute to the notion that the strength of a protein-ligand complex does not only depends on amino acid sequence, topology or unfolding rate constant, but also on the geometry (direction) of the applied force [22,23]. In bacterial populations, we expect differences in the orientation and conformational state of the adhesins, thus differences in the measured forces. The ~1 nN value exceeds by far the typical forces involved in protein-ligand interactions, suggesting an ultrastrong SpsD-elastin interaction, as observed for DLL binding by SdrG [24,25]. Similar bimodal force distributions were observed on SpsL cells (Fig. 2C-D). However, the binding probability dropped from 68 % to 23 % as compared to SpsD cells (Fig. 2D, inset), implying SpsL cells might adhere to elastin through similar mechanism than SpsD but to a much lower extent, barely detectable. To demonstrate the specificity of the probed adhesion forces, we investigated cells lacking both SpsD and SpsL (*ΔspsDΔspsL*) using elastin tips (Fig. S1). Adhesion was abrogated on these mutant cells (3% binding on *n* = 6 cells), showing Sps proteins were exclusively involved in the interaction with elastin.

For both SpsD and SpsL cells, most bonds ruptured ~200 nm, but some distances up to ~800 nm were also observed (see tails in Fig. 2B). It is noteworthy that these long rupture lengths were mainly associated with low forces (< 500 pN), most forces in the nN range breaking ~200 nm. On average, strong forces ruptured at 226 ± 126 nm for SpsD (*n* = 798 data

points), while weak ones were longer-ranged, 307 ± 162 nm, but with many values also in the 400-600 nm range (*n* = 1254) (Fig. 3A,B,E). Similarly, for SpsL cells strong forces did break at 189 ± 123 nm (*n* = 202) and weak ones at 294 ± 160 nm (*n* = 927) (Fig. 3C,D,F). Assuming that the processed mature SpsD and SpsL adhesins comprise 1,031 and 930 residues respectively, that their folded length is about 20 nm and that each amino acid contributes 0.36 nm to the contour length of the polypeptide chain, the fully extended proteins should be ~350 nm and ~315 nm long. This suggests that the adhesins largely extend and unfold in the long-range, low force regime, while they only extend (unfold) moderately in the short-range, high force regime. This intriguing behavior leads us to believe that Sps proteins interact with elastin *via* two interaction mechanisms, likely involving two distinct binding sites. As elastin is firmly attached to the tip via a multi-site chemistry, we expect it to contribute moderately to the observed elongations. However the molecules might be orientated in different ways, and they are known to contain stretchable regions which might therefore contribute, to some extent, to the observed molecular extensions.

Binding of SpsD to elastin is strengthened by mechanical tension. We recently showed that the binding strength of staphylococcal adhesins can be dramatically enhanced by physical force [26,27]. To test whether this applies to SpsD, we studied the dynamics of the interaction, by measuring the adhesion forces while varying the rate at which force is applied (loading rate, *LR*, Fig. 4A). The effective *LR* was estimated from the force *vs* time curves to account for the contribution of the cellular and protein elasticities [28]. We further analyzed force distributions over discrete ranges of *LRs* (Fig. S2). As highlighted in Fig. 4B, the lowest *LR* (< 10,000 pN/s) showed mostly weak forces centered at 108 ± 73 pN while the highest *LR* (> 100,000 pN/s) featured much higher forces of 710 ± 298 pN. At intermediate *LRs*, weak and strong forces coexisted in various proportions. Therefore, the probability of forming strong

bonds increases with the *LR*, implying that the SpsD-elastin interaction strengthens with the applied force. One could argue that strong forces arise from the simultaneous rupture of multiple weak bonds (Fig. 2A and Fig. 4A). However, we did not observe discrete multiples of a specific force unit value, which should be the case in such scenarios. We also looked at the spring constant of the molecular complex (k_m) associated with the low and high forces. The k_m values were obtained using the slope (*s*) of the linear portion of the raw deflection *vs* piezo displacement curves and the following equation: $k_m = (k_c \times s)/(1 - s)$, where k_c is the spring constant of the AFM cantilever. We found that the molecular stiffness increased linearly with the force (Fig. 4C), from 0.004 ± 0.003 N/m (*n* = 476 data points from 3 cells) to 0.024 ± 0.007 (*n* = 321), in the low and high regimes respectively. Hence, the increase in binding strength correlates with an increase in the stiffness of the complex. Together with the difference in rupture lengths, this supports the view that weak and strong interactions are associated with different conformational states of the complex, a soft extended state and a stiff folded state.

Discussion

An interesting feature of the *S. pseudintermedius* SpsD protein is its multi-ligand binding properties, being able to establish interactions with a variety of host extracellular matrix proteins [7]. While Fn-binding by SpsD and elastin-binding by *S. aureus* have been widely investigated, we know very little about the SpsD-elastin interaction. We have shown here that SpsD mediates bacterial adhesion to elastin through weak and strong interactions that depend on mechanical stress.

SpsD binds to elastin with forces (up to 1,500 pN) that largely exceed the typical forces observed in ligand-receptor interactions. SpsL shows such high forces but to a much lower extent, suggesting it may play a different adhesive function. Recently, AFM experiments suggested two distinct contributions for the two adhesins: while SpsL-Fn interactions are

156 weak, facilitating the screening of host cells during colonization, SpsD-Fn interactions are
157 extremely strong allowing the firm attachment of bacteria to the host, even facing high shear
158 stresses. This strong interaction originates from the β-sheet organization of a tandem β-
159 zipper, as previously described for FnBPs of *S. aureus* and *Streptococcus pyogenes* [29,30]. A key
160 difference of the present work is that strong binding is not achieved by a tandem β-zipper but
161 very likely by a DLL mechanism [7], firstly described by Ponnuraj *et al.* for the SdrG-Fg interaction
162 [20]. Supporting this idea, similar strong forces (1 to 2 nN) have been reported for the DLL
163 binding of SdrG, ClfA and ClfB [24–27].

164 The SpsD-elastin interaction strengthens with the tensile force, demonstrating that *S.*
165 *pseudintermedius* adhesion is modulated in response to mechanical stress. Weak binding
166 dominates at low stress, whereas strong binding is favoured at high stress. Perhaps our most
167 intriguing observation is that the transition from weak to strong binding correlates with an
168 increase in molecular stiffness but also with a decrease in molecular extension. Indeed, strong
169 forces are short-ranged and associated with high stiffness, whereas weak ones are of much
170 longer-range and softer.

171 We hypothesize that this finding, never reported for a staphylococcal adhesin, results
172 from two distinct binding mechanisms, regulated by mechanical force (Fig. 5). At low force,
173 elastin would interact with a weak binding site of SpsD, leading to its extension and unfolding,
174 while under high force, conformational changes of the SpsD N2-N3 subdomains would enable
175 elastin to dock in the ligand binding trench and form strong DLL-like interactions. Interestingly,
176 Fg binding by ClfA involves two distinct sites, a DLL interaction between the trench of ClfA N2-
177 N3 subdomains and the extreme C terminus of the γ-chain of Fg [26,31,32], and a second binding
178 site located at the top of the N3 domain.

In conclusion, our experiments suggest that, unlike the SdrG-Fg interaction, Sps proteins interact with elastin via two distinct binding mechanisms, the adhesive function of which is regulated by mechanical tension, following a variant of the DLL mechanism. Our results emphasize that staphylococcal adhesins can engage in a large diversity of force-dependent ligand-binding mechanisms. Finally, this study highlights the ability of numerous pathogens, *S.pseudintermedius* and *S. aureus* included, to process strong molecular interactions with their host ligands, subsequently allowing them to efficiently colonize and infect host cells and biomaterials [33,34].

Methods

Construction of spsD- and spsL-null bacterial mutants and growth conditions. Construction of *spsD*-and spsL-null mutants was performed as previously reported [9]. All strains were grown in Brain Heart Infusion (BHI) broth overnight, at 37°C and under shaking at 200 rpm, to reach their stationary phase. For AFM experiments, cells were harvested by centrifugation at 3,000 *g* for 5 minutes and washed twice with PBS.

Functionalization of AFM cantilevers with elastin. Gold cantilevers (OMCL-TR400PB-1, Olympus Ltd., Tokyo, Japan; nominal spring constant ~ 0.02 N/m) were immersed overnight in an ethanol solution containing 1 mM of 10 % 16- mercaptododecahexanoic acid / 90 % 1-mercapto-1-undecanol (Sigma), rinsed with ethanol and dried with N2. Cantilevers were then immersed for 30 min into a solution containing 10 mg/mL N-hydroxysuccinimide (NHS) and 25 mg/mL 1-ethyl-3-(3- dimethylaminopropyl)-carbodiimide (EDC) (Sigma) and rinsed with ultrapure water. Finally, they were incubated with 0.1 mg/mL of α-elastin, a mixture of soluble peptides obtained from human lung (Calbiochem, Merck, Darmstadt, Germany), for 1 h, rinsed further with PBS buffer, and then immediately used without de-wetting.

Single-molecule force spectroscopy. For SMFS experiments, we used cantilevers with a spring constant of ~0.02 N/m and a resonant frequency of ~2.5 kHz in PBS. They were prepared as described above and bacteria were immobilized on polystyrene substrates. SMFS measurements were performed at room temperature in PBS buffer with a NanoWizard III atomic force microscope (JPK Instruments). Adhesion maps were obtained by recording 32 by 32 force-distance curves on areas of 500 by 500 nm^2 with an applied force of 250 pN, a constant approach and retraction speed of 1,000 nm/s. For loading rate experiments, arrays of 16 by 16 or 32 by 32 force curves were recorded on 500 nm by 500 nm areas at increasing retraction speeds: 0.5, 1, 3, 5 and 10 µm/s. Adhesion force and rupture distance histograms were obtained by calculating the adhesion force and rupture distance of the last peak for each curve. Note that adhesion force values at high retraction speeds might be slightly underestimated by (~5 %) [35]. At least 13 cells of each strain from 3 independent cultures were probed.

Acknowledgements

Work at the Université catholique de Louvain was supported by the European Research Council (ERC) under the European Union's Horizon 2020 research and innovation programme (grant agreement n°693630), the FNRS-WELBIO (grant n°WELBIO-CR-2015A-05), the National Fund for Scientific Research (FNRS), and the Research Department of the Communauté française de Belgique (Concerted Research Action). Funding by the Fondazione CARIPLO (Grant Vaccines 2009-3546) to P.S. is acknowledged. Y.F.D. is Research Director at the FNRS. We thank Ross Fitzgerald for providing mutant strains.

Author Contributions

MMG, CC, FV, PS and YFD designed the experiments, analysed the data and wrote the article. MMG, CC and FV collected the data.

228 Table 1. Probability of adhesion (P_{adh}), adhesion force (F_{adh}) and rupture length (L_{rupt})

229 measured between elastin-modified AFM tips, and SpsD or SpsL cells.

		P_{adh} (%)	Low force regime < 500 pN		High force regime > 500 pN	
			F_{adh} (pN)	L_{rupt} (nm)	F_{adh} (pN)	L_{rupt} (nm)
SpsD	cell 1	79	179 ± 101	209 ± 91	928 ± 399	218 ± 91
	cell 2	44	170 ± 106	158 ± 91	794 ± 268	180 ± 100
	cell 3	50	197 ± 101	370 ± 161	1113 ± 653	316 ± 200
	cell 4	82	244 ± 123	393 ± 193	1082 ± 428	278 ± 157
	cell 5	26	236 ± 121	280 ± 178	1030 ± 450	257 ± 186
	cell 6	95	275 ± 117	331 ± 187	1171 ± 475	256 ± 119
	cell 7	94	296 ± 124	376 ± 189	1201 ± 475	354 ± 113
	cell 8	84	300 ± 136	270 ± 175	844 ± 272	213 ± 118
	cell 9	34	149 ± 94	295 ± 147	1631 ± 576	291 ± 114
	cell 10	83	152 ± 101	376 ± 152	948 ± 384	279 ± 180
	cell 11	87	232 ± 125	271 ± 105	1017 ± 398	233 ± 69
	cell 12	70	155 ± 101	221 ± 85	1027 ± 359	227 ± 73
	cell 13	59	180 ± 118	210 ± 99	997 ± 351	214 ± 76
	cell 14	68	127 ± 80	315 ± 81	893 ± 259	257 ± 152
SpsL	cell 1	16	141 ± 99	150 ± 116	1207 ± 391	110 ± 65
	cell 2	30	144 ± 95	296 ± 193	1393 ± 553	255 ± 186
	cell 3	6	73 ± 16	101 ± 69		
	cell 4	6	62 ± 15	94 ± 55		
	cell 5	12	104 ± 83	231 ± 192		
	cell 6	15	148 ± 111	271 ± 157		
	cell 7	12	113 ± 82	153 ± 73	1367 ± 371	142 ± 79
	cell 8	65	113 ± 44	383 ± 101	874 ± 261	480 ± 312
	cell 9	16	87 ± 54	169 ± 98	1178 ± 204	178 ± 85
	cell 10	54	76 ± 49	371 ± 104	1176 ± 377	182 ± 91
	cell 11	4	82 ± 51	93 ± 30		
	cell 12	25	100 ± 79	440 ± 180	880 ± 323	384 ± 255
	cell 13	39	114 ± 73	182 ± 46	1438 ± 618	322 ± 83

230

References

1 V. Perreten, K. Kadlec, S. Schwarz, U. Grönlund Andersson, M. Finn, C. Greko, A. Moodley, S. A. Kania, L. A. Frank, D. A. Bemis, A. Franco, M. Iurescia, A. Battisti, B. Duim, J. A. Wagenaar, E. van Duijkeren, J. S. Weese, J. R. Fitzgerald, A. Rossano and L. Guardabassi, *J. Antimicrob. Chemother.*, 2010, **65**, 1145–1154.

2 E. van Duijkeren, B. Catry, C. Greko, M. A. Moreno, M. C. Pomba, S. Pyörälä, M. Ruzauskas, P. Sanders, E. J. Threlfall, J. Torren-Edo, K. Törneke and Scientific Advisory Group on Antimicrobials (SAGAM), *J. Antimicrob. Chemother.*, 2011, **66**, 2705–2714.

3 R. Somayaji, M. A. R. Priyantha, J. E. Rubin and D. Church, *Diagn. Microbiol. Infect. Dis.*, 2016, **85**, 471–476.

4 J. A. Geoghegan, E. J. Smith, P. Speziale and T. J. Foster, *Vet. Microbiol.*, 2009, **138**, 345–352.

5 C. Chagnot, A. Listrat, T. Astruc and M. Desvaux, *Cell. Microbiol.*, 2012, **14**, 1687–1696.

6 T. J. Foster, J. A. Geoghegan, V. K. Ganesh and M. Höök, *Nat. Rev. Microbiol.*, 2014, **12**, 49–62.

7 G. Pietrocola, J. A. Geoghegan, S. Rindi, A. Di Poto, A. Missineo, V. Consalvi, T. J. Foster and P. Speziale, *PLoS ONE*, 2013, **8**, e66901.

8 J. Bannoehr, N. L. Ben Zakour, M. Reglinski, N. F. Inglis, S. Prabhakaran, E. Fossum, D. G. Smith, G. J. Wilson, R. A. Cartwright, J. Haas, M. Hook, A. H. M. van den Broek, K. L. Thoday and J. R. Fitzgerald, *Infect. Immun.*, 2011, **79**, 3074–3086.

9 G. Pietrocola, V. Gianotti, A. Richards, G. Nobile, J. A. Geoghegan, S. Rindi, I. R. Monk, A. S. Bordt, T. J. Foster, J. R. Fitzgerald and P. Speziale, *Infect. Immun.*, 2015, **83**, 4093–4102.

10 Biochemistry of tropoelastin - Vrhovski - 1998 - European Journal of Biochemistry - Wiley Online Library, https://febs.onlinelibrary.wiley.com/doi/abs/10.1046/j.1432-1327.1998.2580001.x?sid=nlm%3Apubmed, (accessed March 26, 2020).

11 W. R. Gray, L. B. Sandberg and J. A. Foster, *Nature*, 1973, **246**, 461–466.

12 C. Baldock, A. F. Oberhauser, L. Ma, D. Lammie, V. Siegler, S. M. Mithieux, Y. Tu, J. Y. H. Chow, F. Suleman, M. Malfois, S. Rogers, L. Guo, T. C. Irving, T. J. Wess and A. S. Weiss, *Proc. Natl. Acad. Sci.*, 2011, **108**, 4322–4327.

13 C.-J. Kuo, C. P. Ptak, C.-L. Hsieh, B. L. Akey and Y.-F. Chang, *J. Biol. Chem.*, 2013, **288**, 3886–3896.

14 Y.-P. Lin, D.-W. Lee, S. P. McDonough, L. K. Nicholson, Y. Sharma and Y.-F. Chang, *J. Biol. Chem.*, 2009, **284**, 19380–19391.

15 R. Downer, F. Roche, P. W. Park, R. P. Mecham and T. J. Foster, *J. Biol. Chem.*, 2002, **277**, 243–250.

16 P. W. Park, T. J. Broekelmann, B. R. Mecham and R. P. Mecham, *J. Biol. Chem.*, 1999, **274**, 2845–2850.

17 F. M. Roche, R. Downer, F. Keane, P. Speziale, P. W. Park and T. J. Foster, *J. Biol. Chem.*, 2004, **279**, 38433–38440.

18 F. M. Keane, A. W. Clarke, T. J. Foster and A. S. Weiss, *Biochemistry*, 2007, **46**, 7226–7232.

19 F. M. Keane, A. Loughman, V. Valtulina, M. Brennan, P. Speziale and T. J. Foster, *Mol. Microbiol.*, 2007, **63**, 711–723.

20 K. Ponnuraj, M. G. Bowden, S. Davis, S. Gurusiddappa, D. Moore, D. Choe, Y. Xu, M. Hook and S. V. L. Narayana, *Cell*, 2003, **115**, 217–228.

21 Y. F. Dufrêne and A. Persat, *Nat. Rev. Microbiol.*, 2020, 1–14.

22 D. J. Brockwell, E. Paci, R. C. Zinober, G. S. Beddard, P. D. Olmsted, D. A. Smith, R. N. Perham and S. E. Radford, *Nat. Struct. Biol.*, 2003, **10**, 731–737.
23 S. M. Sedlak, L. C. Schendel, M. C. R. Melo, D. A. Pippig, Z. Luthey-Schulten, H. E. Gaub and R. C. Bernardi, *Nano Lett.*, 2019, **19**, 3415–3421.
24 L. F. Milles, K. Schulten, H. E. Gaub and R. C. Bernardi, *Science*, 2018, **359**, 1527–1533.
25 P. Herman, S. El-Kirat-Chatel, A. Beaussart, J. A. Geoghegan, T. J. Foster and Y. F. Dufrêne, *Mol. Microbiol.*, 2014, **93**, 356–368.
26 P. Herman-Bausier, C. Labate, A. M. Towell, S. Derclaye, J. A. Geoghegan and Y. F. Dufrêne, *Proc. Natl. Acad. Sci.*, 2018, **115**, 5564–5569.
27 P. Vitry, C. Valotteau, C. Feuillie, S. Bernard, D. Alsteens, J. A. Geoghegan and Y. F. Dufrêne, *mBio*, 2017, **8**, e01748-17.
28 D. Alsteens, M. Pfreundschuh, C. Zhang, P. M. Spoerri, S. R. Coughlin, B. K. Kobilka and D. J. Müller, *Nat. Methods*, 2015, **12**, 845–851.
29 U. Schwarz-Linek, S. Gurusiddappa, J. H. Kim, E. S. Pilka, J. A. G. Briggs, T. S. Gough, I. D. Campbell and J. R. Potts, 2003, **423**, 5.
30 V. Prystopiuk, C. Feuillie, P. Herman-Bausier, F. Viela, D. Alsteens, G. Pietrocola, P. Speziale and Y. F. Dufrêne, *ACS Nano*, 2018, **12**, 3609–3622.
31 V. K. Ganesh, X. Liang, J. A. Geoghegan, A. L. V. Cohen, N. Venugopalan, T. J. Foster and M. Hook, *EBioMedicine*, 2016, **13**, 328–338.
32 V. K. Ganesh, J. J. Rivera, E. Smeds, Y.-P. Ko, M. G. Bowden, E. R. Wann, S. Gurusiddappa, J. R. Fitzgerald and M. Höök, *PLOS Pathog.*, 2008, **4**, e1000226.
33 L. F. Milles and H. E. Gaub, *Curr. Opin. Struct. Biol.*, 2020, **60**, 124–130.
34 M. Mathelié-Guinlet, F. Viela, A. Viljoen, J. Dehullu and Y. F. Dufrêne, *Curr. Opin. Biomed. Eng.*, 2019, **12**, 1–7.
35 M. R. Uhlig, C. A. Amo and R. Garcia, *Nanoscale*, 2018, **10**, 17112–17116.

Figure legends

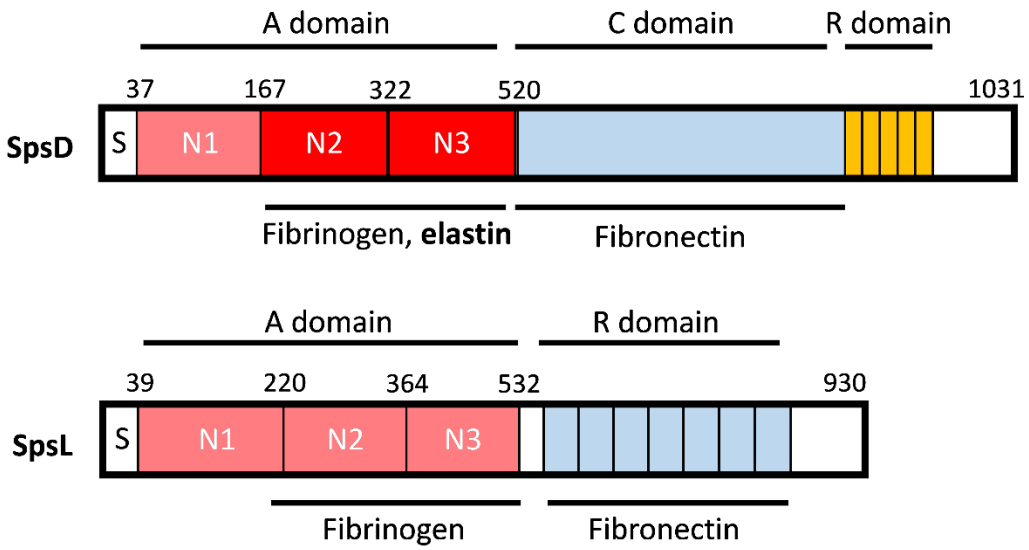

Figure 1. Schematic diagram of the domain organization of SpsD and SpsL. The A domain of SpsD spans residues 37 to 519 following the signal sequence (S). This is followed by a connecting region C (residues 520-866) and a repeat region R. A sorting signal (SS) containing a LPXTG motif, a hydrophobic domain and a positively charged stretch occurs at the extreme C-terminus. SpsL includes a signal sequence (S) at the N-terminus, followed by an A domain (aa 39-531), a R domain containing seven tandem repeats (aa 543-818) and a C-terminal sorting signal (SS).

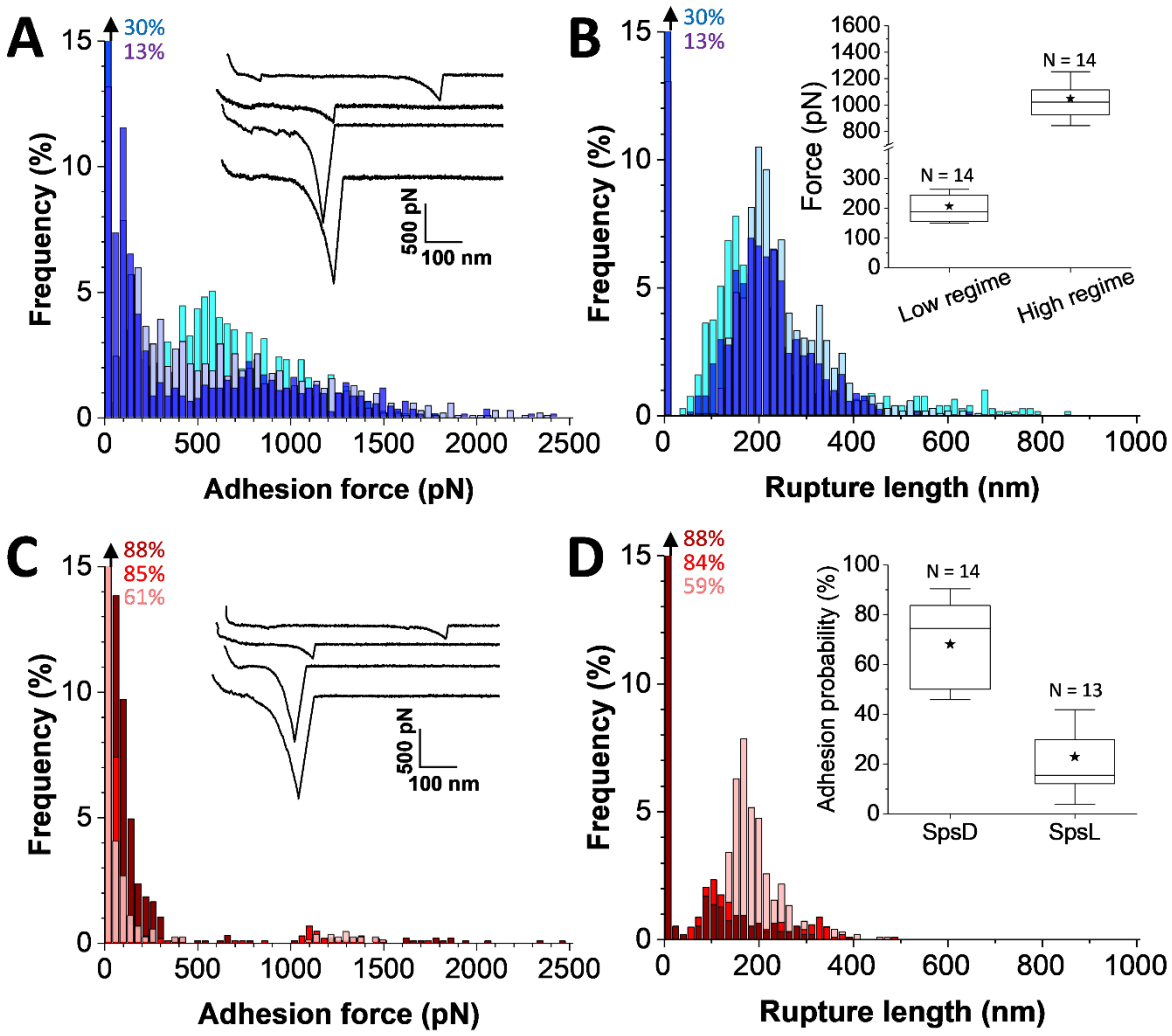

315

316 **Figure 2. Binding strength of single SpsD and SpsL adhesins on living bacteria.** (*A-D*)
317 Maximum adhesion force (A, C) and rupture length histograms (B, D) obtained by recording
318 force-distance curves in PBS between three different *S. pseudintermedius* SpsD cells (A, B) or
319 SpsL cells (C, D) and AFM tips functionalized with elastin, at a constant retraction speed of 1
320 µm/s (*LR* of about 2.10^4 pN/s). Percentages shown in the upper left corners of the histograms
321 correspond to the fraction of non-adhesive events. Left insets show representative retraction
322 force profiles. Right insets show the average forces obtained among 14 independent SpsD cells
323 in the low and high force regimes (B) and statistical analysis of the binding probability of SpsD
324 and SpsL cells to elastin (D). Stars represent the mean values, the box the 25% - 75 % quartiles
325 and the error bars the standard deviation among N independent cells.

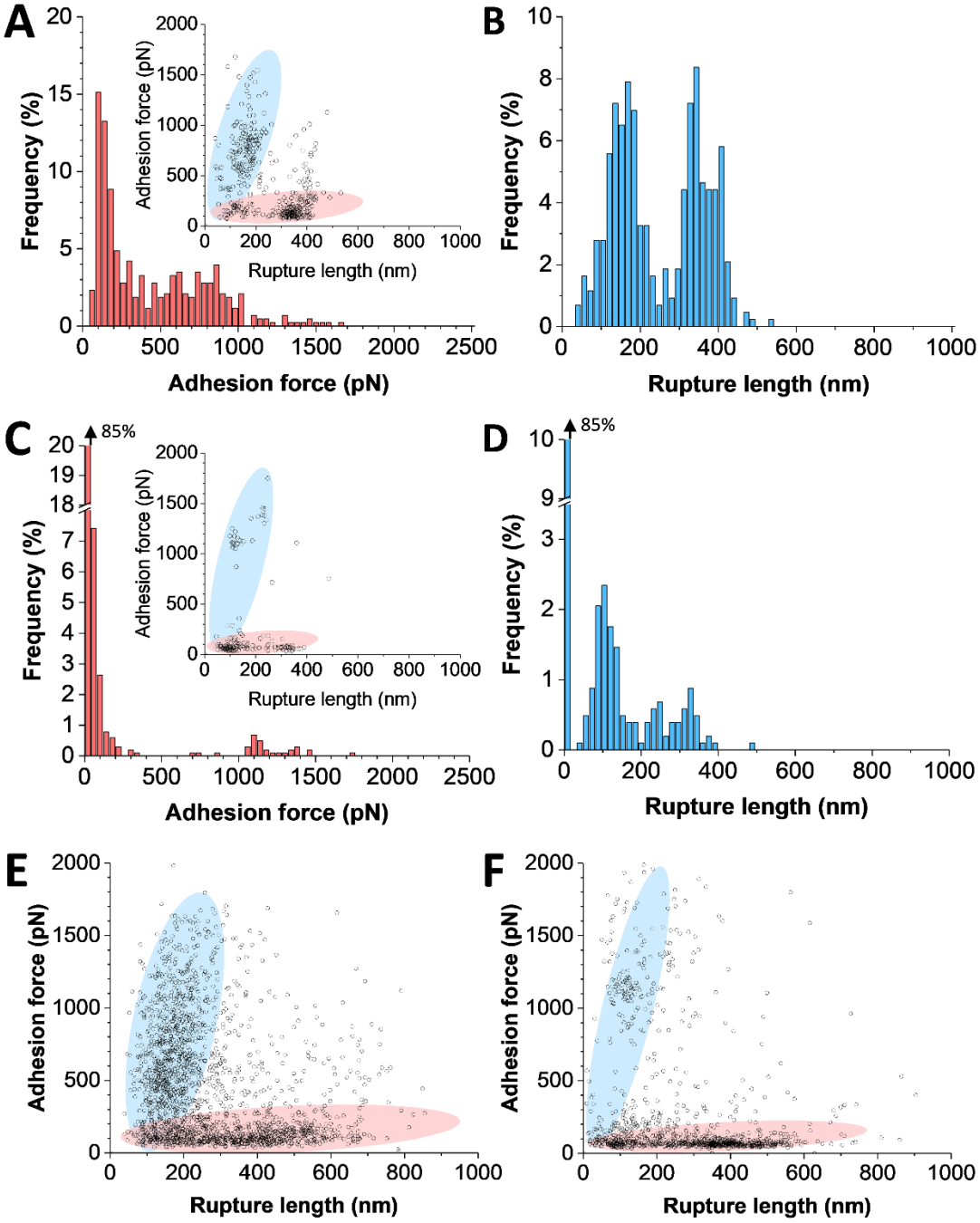

Figure 3. The binding strengths and rupture lengths of SpsD (and SpsL) are inversely correlated. Maximum adhesion force (A, C) and rupture length histograms (B, D) obtained for one SpsD cell (A,B) and one SpsL cell (C, D), and (inset) corresponding plot of adhesion forces *versus* rupture lengths (n = 430 and n = 159 data points for SpsD and SpsL respectively). (E-F) Plots of adhesion forces *versus* rupture lengths for three independent SpsD and SpsL cells (n = 2,052 and n = 1,129 data points for SpsD and SpsL, respectively).

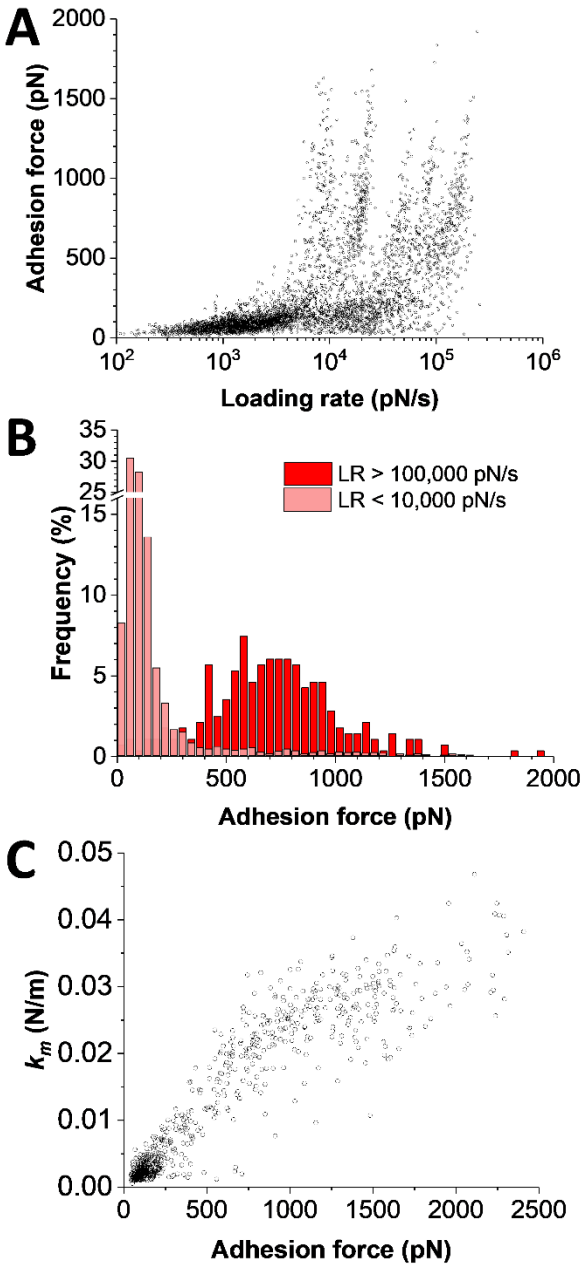

333

334 **Figure 4. SpsD binds elastin through a force-dependent mechanism.** (A) Dynamic force
335 spectroscopy plot obtained by recording force-distance curves in PBS between elastin-tips and
336 SpsD cells (n = 4,424 data points from five independent cells). (B) Adhesion force distribution
337 at low and high loading rates (LRs), highlighting the shift towards higher forces with increasing
338 stress. (C) Scatter plot of the spring constants of the molecular complex (k_m) vs adhesion forces
339 showing the switch to higher stiffness at high forces (n = 797 data points from three
340 independent cells).

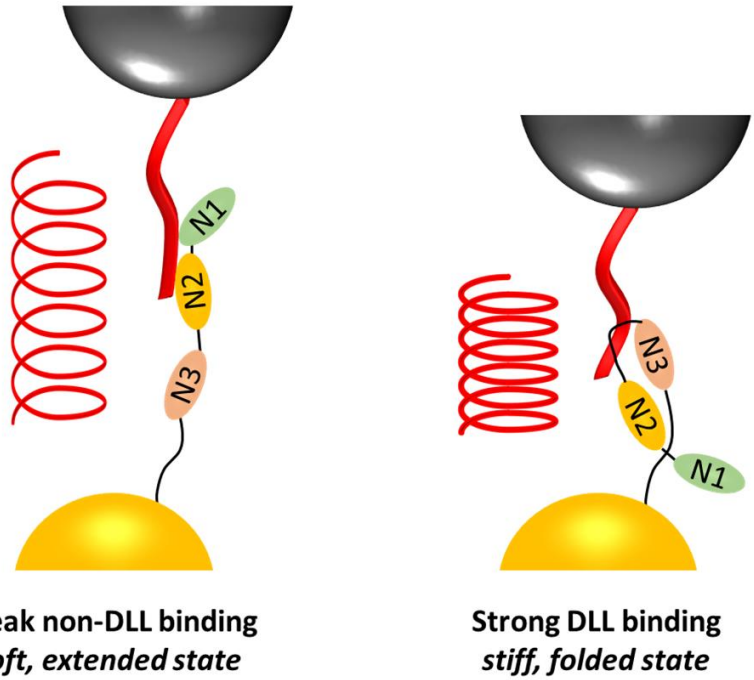

341

342 **Figure 5. Proposed model for the force-dependent dual interaction of SpsD.** The stiff, strong

343 and short-ranged interaction arises from the DLL binding of elastin within the trench formed

344 by the N2-N3 subdomains (right), whereas the soft, weak and extended interaction involves

345 adhesion of elastin to a weak, non-DLL binding site of SpsD.